Metabolic labeling of hyaluronan: Biosynthesis and quantitative analysis of ^{13}C,^{15}N-enriched hyaluronan by NMR and MS-based methods

Yan Xue [a,*], Karolina Ucieklak [b], Suresh Gohil [a], Tomasz Niedziela [b], Gustav Nestor [a], Corine Sandström [a]

[a] Department of Molecular Sciences, Uppsala BioCenter, Swedish University of Agricultural Sciences, P.O. Box 7015, SE-750 07, Uppsala, Sweden
[b] Hirszfeld Institute of Immunology and Experimental Therapy, 53-114, Wroclaw, Poland

ABSTRACT

Hyaluronan (HA), a member of the GAG family of glycans, has many diverse biological functions that vary a lot depending on the length of the HA chain and its concentration. A better understanding of the structure of different-sized HA at the atomic level is therefore crucial to decipher these biological functions. NMR is a method of choice for conformational studies of biomolecules, but there are limitations due to the low natural abundance of the NMR active nuclei ^{13}C and ^{15}N. We describe here the metabolic labeling of HA using the bacterium *Streptococcus equi* subsp. *Zooepidemicus* and the subsequent analysis by NMR and mass spectrometry. The level of ^{13}C and ^{15}N isotope enrichment at each position was determined quantitatively by NMR spectroscopy and was further confirmed by high-resolution mass spectrometry analysis. This study provides a valid methodological approach that can be applied to the quantitative assessment of isotopically labeled glycans and will help improve detection capabilities and facilitate future structure-function relationship analysis of complex glycans.

1. Introduction

Hyaluronic acid (HA) is a highly anionic polysaccharide in the glycosaminoglycan (GAG) family with a linear non-sulfated chain built of *N*-acetyl glucosamine (GlcNAc) and glucuronic acid (GlcA) in the repeating disaccharide unit →4)-D-Glc*p*A-β(1→3)-D-Glc*p*NAc-β(1→ (Fig. 1). HA chains can be intertwined to form highly viscous and elastic solutions at very low concentrations [1]. Due to the unique viscoelasticity and strong anionic nature, HA acts as a lubricant and space-filling molecule to protect adjacent tissues and contributes to tissue hydration and osmotic balance [2]. HA is present in vertebrate tissues and fluids with diverse physiological roles: it contributes to homeostatic control of intracellular signaling pathways in proliferation, adhesion, differentiation and migration, and in tissue morphogenesis [3,4]. Although the primary structure of HA is deceptively simple, its biological functions are highly complex. As an essential component of the extracellular matrix (ECM), the structure-function relationships of HA are difficult to establish due to the complexities arising from its variable chain length, concentration, interactions with HA binding proteins, and biosynthesis *versus* enzymatic degradation [5,6]. As a result, HA has different and sometimes contradictory effects on many biological functions, for example, the differential distribution of HA in tissues varies at individual developmental stages and pathological conditions [3]; moreover,

different molecular weights of HA have conflicting effects on the regulation of macrophage activation: low-molecular-weight HA has a pro-inflammatory response, while high-molecular-weight HA has an anti-inflammatory response [7]. Therefore, a deeper understanding of the structure of HA at the atomic level is crucial and helps to provide new insights into its biological roles.

Nuclear magnetic resonance (NMR) spectroscopy is a powerful characterization method that provides detailed information on the structure at atomic-resolution of biomolecules, as well as on protein-carbohydrate interactions [8]. However, carbohydrate NMR suffers from poor chemical-shift dispersion in 1D ^{1}H experiments due to spectral overlap. Heteronuclear NMR experiments, which take advantage of the larger spectral dispersion of ^{13}C and ^{15}N, have lower sensitivity due to the low natural abundance of these NMR-active nuclei. To address these issues, optimized multidimensional NMR experiments with improved resolution in both ^{1}H and ^{13}C dimensions have been applied to resolve the overlap of glycan signals [9,10]. Another rapidly evolving technique is isotopic labeling, which not only enables a significant sensitivity enhancement and fast acquisition of the NMR experiments, but it also allows for detection of precise contact points between interacting molecules [11,12]. The use of isotope-filtered or isotope-edited experiments on ^{13}C-labeled sugars in protein complexes has enabled tailored identification of inter-molecular NOEs [11] as well as sugar

Fig. 1. Schematic representation of HA polysaccharide built by repeating disaccharide unit of →4)-D-Glc*p*A-β(1→3)-D-Glc*p*NAc-β(1→ (left) and ΔHA₂ obtained by degradation with chondroitinase ABC (right).

hydroxyl protons involved in hydrogen bonds with the protein [13]. Such experiments have been used more often on protein-ligand interactions in general [14] and on protein-RNA interactions [15], but an easier access to ^{13}C-labeled glycans has the potential for a more frequent use of these experiments on protein-glycan interactions [16].

In recent years, NMR spectroscopists and glycoscientists have started to explore the development of new isotope labeling methods. The preparation of ^{13}C and/or ^{15}N enriched heparin, its precursors and unsulfated chondroitin from *E. coli* K5 has been reported [17–20], as well as the *in vivo* ^{15}N -labeling of GAG oligosaccharides [21]. Glycoproteins containing uniformly and site-specifically ^{13}C-enriched *N*-acetylneuraminic acid have been produced and NMR pulse sequences tailored for sialylated biomolecules were reported [22]. Furthermore, ^{15}N NMR has been exploited on oligomers of glycosaminoglycan, which resulted in resolved NH signals owing to the enhanced chemical shift dispersion in ^{15}N compared to ^{1}H [23,24]. The use of ^{15}N labeling together with ^{13}C labeling not only enables ^{15}N-edited 3D NMR experiments to resolve resonance overlap but also provides valuable sequence-specific information of the inter-residues of nitrogen-containing glycans. However, the use of isotope labeling methods to establish structural information from glycan is still very limited compared to the widespread applications of isotope labeling in protein NMR.

Since the 1980s, microbial-derived biotechnology has been developed for the production of HA. Among the bacteria capable of synthesizing HA, there are both Gram-positive Streptococci of groups A and C (e.g. *Streptococcus equi* subsp. *zooepidemicus*) and Gram-negative pathogenic bacteria (e.g. *Pasteurella multocida*). In comparison with previously reported *E. coli* K5 strain transfected with the recombinant HA synthase from *Pasteurella multocida*, *Streptococcus equi* subsp. *Zooepidemicus* is a natural producer of HA as a capsule of the bacteria and it is commonly used in a variety of culturing protocols employed for the biotechnological production of HA. Therefore, it allows to exploit the native biosynthetic pathways of *Streptococci* for the production of HA, using ^{13}C- and ^{15}N-labeled substrate replacement in the culturing medium. The prevalence in the biotechnological applications, the ease of isolation, and a relatively high yield of the obtained HA made the *Streptococcus zooepidemicus* the optimal bacterium for the purposed approach of isotopic labeling.

We herein report on the biosynthetic production of ^{13}C,^{15}N-labeled HA polysaccharides by *Streptococcus zooepidemicus* using small-scale cultures and media with defined carbon and nitrogen sources. The isotopic distribution and the extent of isotopic enrichment of the labeled HA polysaccharide were assessed quantitatively by NMR and mass spectrometry (MS). Performing analysis on intact HA polymer of high molecular weight is difficult or even not feasible due to high viscosity that leads to poor sensitivity and severe line broadening of NMR resonances resulting in inaccurate signal integration. Therefore, the polysaccharide was enzymatically digested to disaccharide prior to NMR and MS analysis. This study provides a valid methodological approach that can be applied to the quantitative assessment of isotopically labeled glycans and will help improve detection capabilities and facilitate future structure-function relationship analysis of complex glycans.

2. Results and discussion

2.1. Biosynthesis of isotopically labeled HA polysaccharide

For the production of the bio-synthetically ^{13}C and ^{15}N-labeled HA, *Streptococcus equi* subsp. *Zooepidemicus* - a bacterium that is commonly used in the biotechnological production of HA was employed. The biosynthesis pathways of HA have already been well-established: glucose in the source medium enters the bacterial metabolic pathways through enzymatic conversion to glucose-6-phosphate, followed by isomerization to fructose-6-phosphate. The fructose-6-phosphate is directly involved in the synthesis of acetamido sugars using L-glutamine as the source of amine and an acetyl-CoA as a source of the *N*-acetyl group [25]. Thus, GlcA and GlcNAc are derived from glucose-6-phosphate and fructose-6-phosphate, respectively, and UDP-GlcNAc and UDP-GlcA become the direct precursors of HA [26]. However, the synthesis of HA competes constantly with cell growth. The metabolic pathways of glucose provide also the building blocks that constitute bacterial cell wall polysaccharides, teichoic acids, and bacterial biomass in general. Consequently, only 10% of the initial glucose ends up in HA [27]. The metabolic labeling used in this study relied on the initial assumptions that, first, glucose is a primary carbon source for both D-GlcA and D-GlcNAc during the HA biosynthesis; second, L-glutamine provides the amino group for the Glc-6-P→Fru-6-P→GlcN-6-P conversion pathway that leads to D-GlcNAc formation; and third, the complete replacement of D-glucose and L-glutamine in the medium with U–^{13}C₆-D-glucose and L-glutamine-(amide-^{15}N) should yield the ^{13}C,^{15}N-labeled HA.

2.2. Isolation of ^{13}C,^{15}N-enriched ΔHA₂

The HA polysaccharide was digested using chondroitinase ABC. This lyase can cleave via a *β*-elimination reaction all 1 → 4 linkages between GlcNAc and GlcA to generate the disaccharide ΔHA₂ with an unsaturated uronic acid at the non-reducing end [28,29] (Fig. 1). The products of the digestion were fractionated by HPLC and the α and β anomers of the disaccharides were well separated as two chromatographic peaks (Fig. S1). The fractions containing ΔHA₂ were lyophilized and further analyzed by NMR spectroscopy and MS.

2.3. NMR analyses of ^{13}C,^{15}N-enriched ΔHA₂

2.3.1. Chemical shift assignment
The ^{1}H, ^{13}C, and ^{15}N resonances of ΔHA₂ were assigned from a series of 1D and 2D NMR experiments including ^{1}H,^{13}C-HSQC, ^{1}H,^{15}N-HSQC, and ^{1}H,^{13}C-HMBC. The data are in good agreement with previously published results on HA oligosaccharides [23,30,31]. In aqueous solution, the GlcNAc reducing end of ΔHA₂ is present in equilibrium between the α- and β-anomers in a 62/38% ratio due to mutarotation. Therefore, signals arising from both α- and β-anomers should be observed for all protons and carbons on both the reducing and non-reducing sugars. However, due to the negligible effect of anomeric configuration on the neighboring sugar and the limited spectral resolution, the ^{1}H and ^{13}C signals for the α- and β-form of the disaccharide
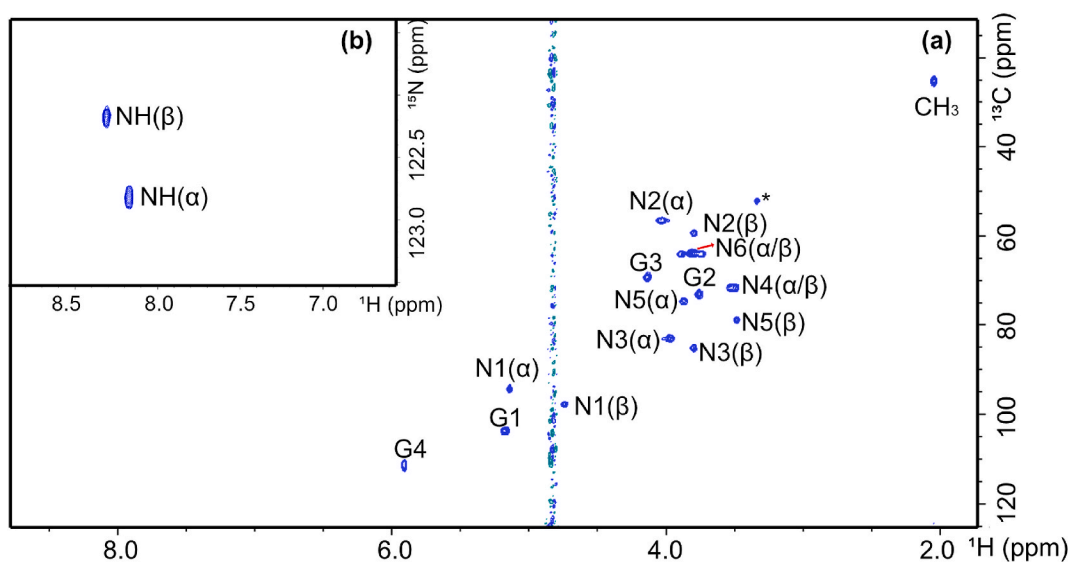
Fig. 2. 2D (a) ^{1}H,^{13}C-HSQC and (b) ^{1}H,^{15}N-HSQC spectra of ^{13}C,^{15}N-enriched ΔHA$_2$ at 25 °C. Cross-peaks are annotated with **G** representing GlcA and **N** representing GlcNAc followed by a number indicating the position giving rise to the signal. NH and CH$_3$ represent signals arising from the amide and methyl protons of the *N*-acetyl group on GlcNAc, respectively. α and β represent the anomeric configuration of GlcNAc. *: Methanol.

can only be differentiated on the reducing sugar as shown in Fig. 2a. Similarly, the amide proton cross-peaks of α- and β-anomers could be identified in the ^{1}H,^{15}N-HSQC spectrum (Fig. 2b).

2.3.2. Quantitative NMR analysis

The level of isotope enrichment in ΔHA$_2$ was determined from a combination of 1D and 2D quantitative NMR experiments. Since data reliability in quantitative NMR analysis is influenced by many factors, such as the relaxation delay, NOE, signal-to-noise ratio (S/N), and digitization, the acquisition and processing parameters must be treated with caution. Based on previous relaxation time measurements [32–34], a relaxation delay of 25 s was chosen for both ^{1}H and ^{13}C experiments to ensure complete nuclear relaxation, and 16 k scans were acquired for ^{13}C experiments to obtain a sufficient S/N. In addition, quantitative determination of isotopic enrichment in a commercially purchased [UL-^{13}C$_8$; ^{15}N]-GlcNAc sample was conducted to validate our NMR methods based on 1D ^{1}H, 1D^{13}C, and 2D ^{1}H,^{13}C-HSQC (see more information in Experimental and Supporting Information).

The characteristic amide proton (δ 8.0–8.5 ppm) and methyl protons (δ 1.8–2.1 ppm) of the *N*-acetyl group of GlcNAc and the G4 proton (δ 5.5–6.0 ppm) of ΔGlcA can be differentiated from the other overlapping

signals in the 1D ^{1}H spectrum (Fig. 3, highlighted in red). However, signals from protons bound to unlabelled nuclei (i.e., ^{12}C and ^{14}N) and labeled nuclei (^{13}C and/or ^{15}N) are observed simultaneously. Therefore, three ^{13}C- or ^{15}N-decoupled ^{1}H NMR spectra were acquired to distinguish between the ^{1}H signals of isotopically labeled and unlabelled ΔHA$_2$ (Fig. 3a, b, and c). In Fig. 3a, the ^{1}H spectrum with ^{15}N decoupling shows two doublets at 8.32 and 8.18 ppm, corresponding to the amide proton of β- and α-GlcNAc, respectively. Without ^{15}N decoupling, the two doublets are split and partially overlapped due to the ^{1}H–^{15}N one-bond *J*-coupling. The signals from the proton bound to ^{14}N without splitting from the ^{1}H–^{15}N coupling show incomplete ^{15}N incorporation

Table 1
Mean level of isotope enrichment (%) of ^{13}C and ^{15}N in ΔHA$_2$ determined by quantitative ^{1}H NMR.[a].

Proton positions		
G4	NH (α/β)	Me
96 ± 2	66 ± 1/63 ± 2	61 ± 2

[a] Data with standard deviation are presented from at least three measurements and D1 was set to 25 s.
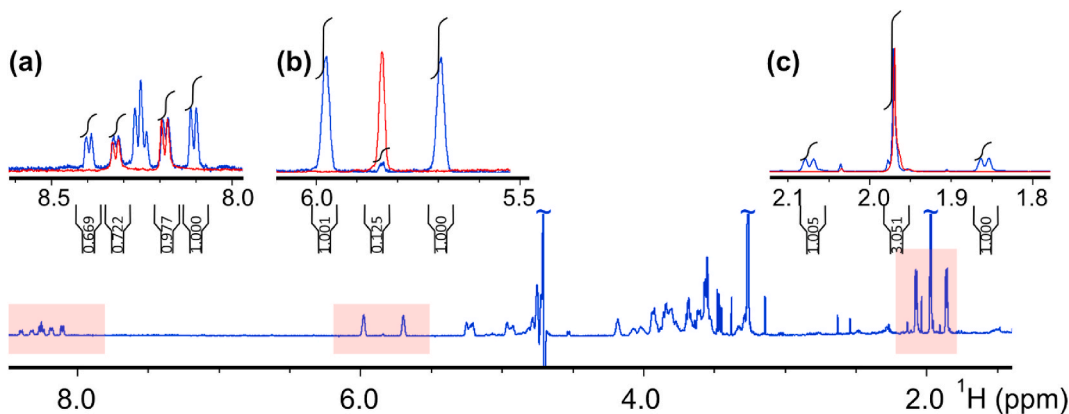
Fig. 3. 1D ^{1}H NOESY presaturation spectrum (blue) of ^{13}C,^{15}N-enriched ΔHA$_2$ at 25 °C. Highlighted regions correspond to (a) amide protons with ^{15}N decoupling centered at 120 ppm (red); (b) G4 proton with ^{13}C decoupling centered at 110 ppm (red); (c) methyl protons with ^{13}C decoupling centered at 30 ppm (red). The intensity of decoupled spectra was adjusted to match the NOESY presaturation spectrum. The water suppression was achieved by presaturation during relaxation delay (d1 = 25s) and mixing time (d8 = 50 ms).
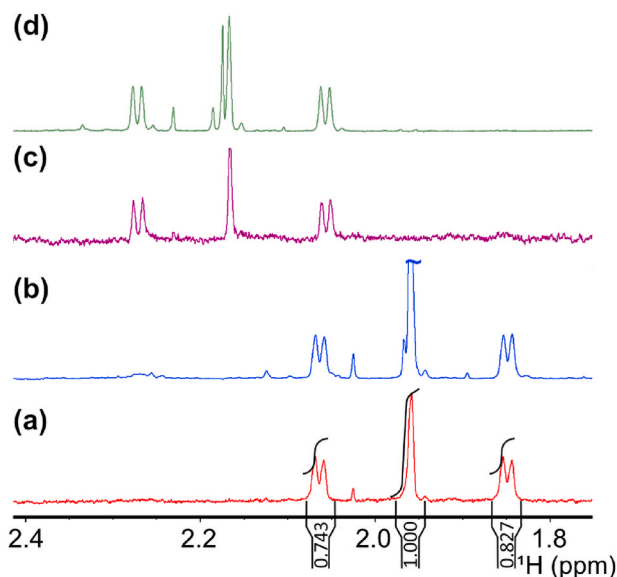
Fig. 4. 1D diffusion NMR of $^{13}C,^{15}N$-enriched ΔHA_2 with 95% gradient strength at (a) 25 °C and (c) 45 °C and 1D NOESY presaturation at (b) 25 °C and (d) 45 °C. 1D diffusion experiments filtered out the signals of low-molecular-weight impurities lying around the methyl signal at 1.97 ppm. Two impurity signals superimposed with the methyl signal at 25 °C could be separated at 45 °C (Fig. 4d).

at the acetamido group. By integrating the NH proton signals in the 1D ^1H spectrum without ^{15}N decoupling (^1H–^{14}N and ^1H–^{15}N signals, respectively), the average level of ^{15}N isotope enrichment was estimated to be 66% from the NH signal associated with the α anomer and 63% from the NH signal associated with the β anomer (Table 1). In Fig. 3b, the ^1H spectrum with ^{13}C decoupling has a singlet at 5.84 ppm,

corresponding to the G4 proton. The singlet is split by the $^1J_{CH}$ coupling when recorded in the absence of ^{13}C decoupling. However, a minor signal remains at 5.84 ppm, which corresponds to the proton bound to ^{12}C and which therefore shows incomplete ^{13}C incorporation on the GlcA pyranose ring. Integration of the signals gave an average level of ^{13}C isotope enrichment on G4 of 96% (Table 1).

Using the same approach, the level of ^{13}C isotope enrichment on the methyl group was determined to be 40% by integrating the ^1H–^{12}C signal and the ^1H–^{13}C signal split by $^1J_{CH}$ respectively (Fig. 3c). This value was significantly lower than the one obtained from quantitative 1D ^{13}C and 2D $^1H,^{13}C$-HSQC NMR experiments and from MS data (*vide infra*). This discrepancy was due to the presence of traces of two impurities lying under the methyl signal at 1.97 ppm as demonstrated by 1D ^1H diffusion experiments that filter out signals from low molecular weight compounds as well as 1D ^1H spectra recorded at several temperatures. (see Fig. 4 for details). The average level of isotope enrichment of ^{13}C on the methyl group was then determined by 1D diffusion experiments to be about 61%.

Quantitative 1D ^{13}C NMR experiments were then performed to determine the extent of ^{13}C incorporation in ΔHA_2 (Fig. 5). The integration values at each carbon site are listed in Table 2. The discrepancies obtained by 1D ^{13}C NMR are attributed in part to the low S/N ratio due to the small amount of sample, which is more pronounced for the N2 position of GlcNAc (see Fig. 5). Quantitative HSQC experiments were also performed to further corroborate the ^{13}C results (Table S1). The intensity of cross-peaks in 2D HSQC is not directly proportional to the concentration but is highly signal specific and is affected by several different parameters such as T_1 and T_2 relaxation times, off-resonance effects, $^1J_{CH}$ coupling, J_{HH} couplings, and peak multiplicity [35–37]. In addition, ^{13}C-labeled compounds introduce the effect of $^1J_{CC}$ couplings, which evolve when magnetization has been transferred to ^{13}C and will affect the relative intensities. Similarly, ^{13}C decoupling could have an impact on the intensity of HSQC cross-peaks, especially for ^{13}C-labeled compounds [38]. Therefore, the quantitative HSQC results
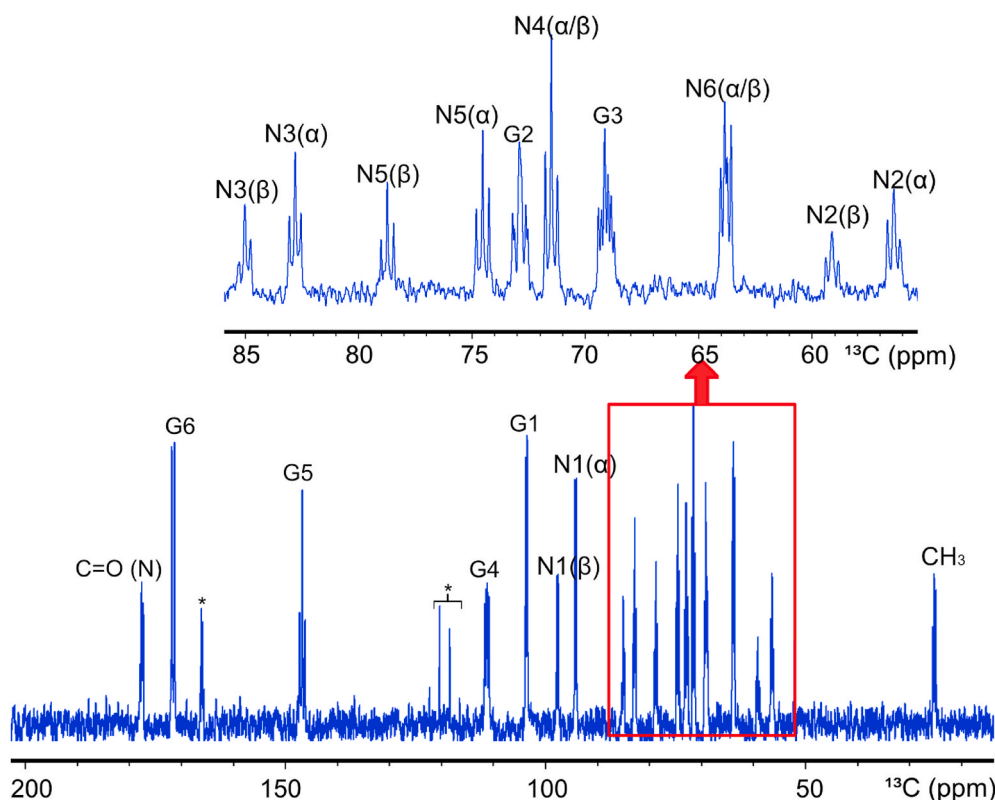
Fig. 5. 1D ^{13}C NMR spectrum of $^{13}C,^{15}N$-enriched ΔHA_2 at 25 °C. *: Trifluoroacetic acid (TFA).

Table 2
Mean level of isotope enrichment (%) of ^{13}C at each carbon of ΔHA_2 determined by quantitative ^{13}C NMR.[a]

| | ^{13}C isotope enrichment (%) at carbon positions | | | | | | | |
	C-1	C-2	C-3	C-4	C-5	C-6	CO	Me
ΔGlcA	100 $\pm$ 10	89 $\pm$ 1	90 $\pm$ 4	97 $\pm$ 8	87 $\pm$ 1	100[b]	/	/
GlcNAc $(\alpha+\beta)$	90 $\pm$ 10	77 $\pm$ 3	86 $\pm$ 5	83 $\pm$ 1	90 $\pm$ 8	100 $\pm$ 4	59 $\pm$ 1	64 $\pm$ 3

[a] Data with standard deviation are presented from at least two measurements and D1 was set to 25 s.

[b] The integration value was set as a reference.

were used as additional experimental data, while the 1D ^{13}C NMR data provided more reliable quantitative measurements. However, inspection of Table 2 and Table S1 shows relatively good agreement between data obtained from 1D ^{13}C NMR and 2D HSQC.

Thus, the isotopic purity of ^{13}C in the two pyranose rings was determined to be 80–100%. Since glucose is the primary carbon source for both GlcA and GlcNAc during HA biosynthesis, it is expected that all carbon within a sugar ring will have the same amount of ^{13}C enrichment and the range of ^{13}C enrichment 80–100% obtained for the different carbon atoms must be therefore inherent to errors from the ^{13}C NMR measurements.

For the *N*-acetyl group, the level of isotope enrichment of both ^{13}C and ^{15}N was determined to be 60–65%, which may be due to isotopic dilution during the acetylation of glucosamine-1-phosphate, resulting in incomplete ^{13}C and ^{15}N incorporation [39].

2.4. MS analysis of $^{13}C,^{15}N$-enriched ΔHA_2

$^{13}C,^{15}N$ incorporation and their isotopic distribution in the isolated ΔHA_2 product were also assessed by ESI-orbitrap-MS in addition to NMR analyses. ESI-orbitrap-MS revealed a cluster of peaks of protonated molecular ions ([M+H]$^+$) from m/z 395 to 391 in the extracted ion chromatogram (EIC) (Fig. 6a). A distinct peak was present at m/z 395.1620 corresponding to [UL-$^{13}C_{14}$; ^{15}N]- ΔHA_2. The different mass shifts that occur in the nearby region correspond to combinations of isotopic variants. By amplifying the mass shift regions (m/z 392, 393, and 394, respectively), two peaks with different m/z values can be found at each site (dash boxes in Fig. 6a). The mass difference between the uniformly labeled peak and the remaining peaks was first calculated, after which the isotopologue of each peak was assigned by comparing the mass differences between ^{15}N and ^{14}N (0.9970 Da), and ^{13}C and ^{12}C (1.0034 Da) as shown in Fig. 6b. The observed m/z values, the measured and expected mass differences, the relative percentage of each peak, as well as the isotopologues are also summarized in Table 3. The maximum deviation of the measured and expected mass difference is 1.5×10^{-3} Da, which can be explained by the very low abundance of the peak and the limited number of data points used for curve fitting.

In summary, the fully $^{13}C,^{15}N$-labeled ΔHA_2 peak at m/z 395.1620 accounted for 37.8% of the total. The neighboring peak at m/z 394.1649 corresponds to the complete ^{13}C incorporation (one ^{15}N loss) of ΔHA_2, accounting for 19.4% of the total. Adding these two peaks together, the percentage of complete ^{13}C incorporation of ΔHA_2 should be at least 57.2% ($\geq$37.8% + 19.4%). This is in good agreement with our conclusion from quantitative NMR that the ^{13}C level of isotope enrichment of
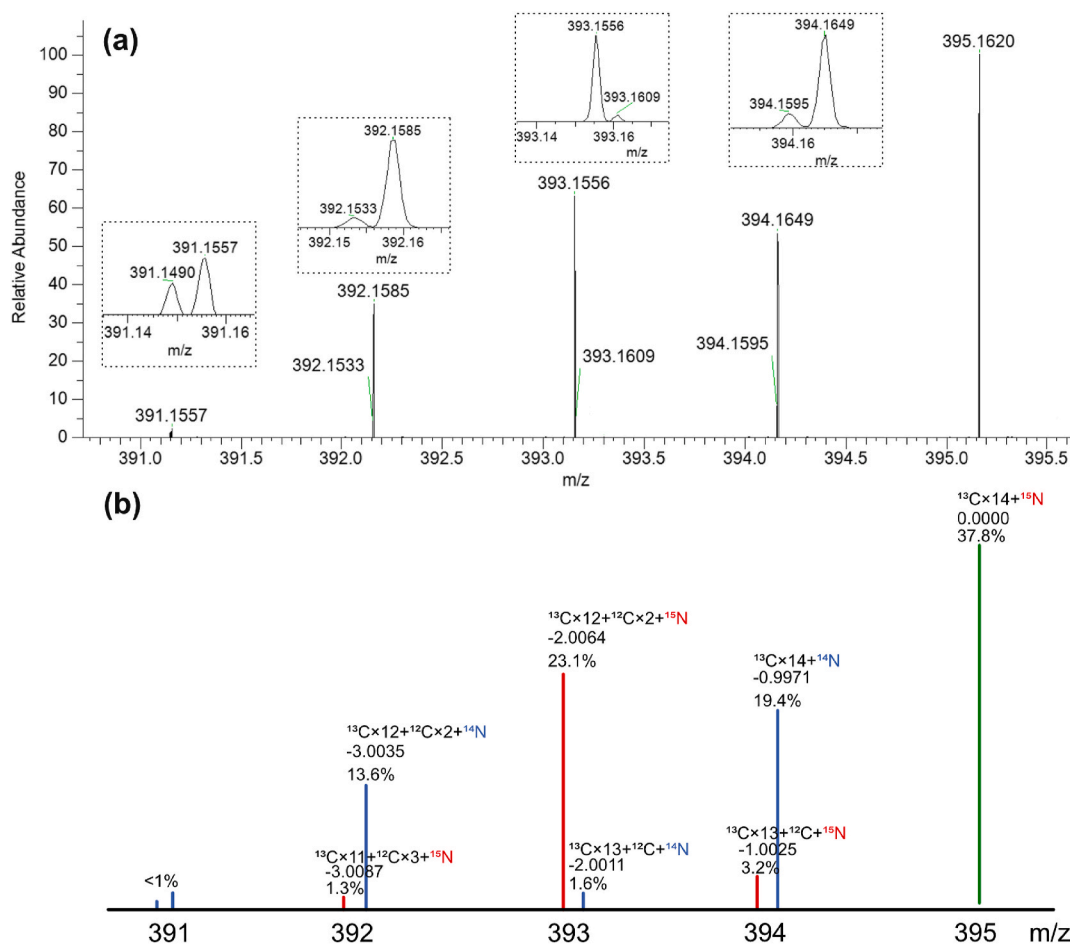
Fig. 6. (a) ESI-orbitrap-MS [M+H]$^+$ spectrum of $^{13}C,^{15}N$-enriched ΔHA_2; amplified mass shift regions are shown in the dash boxes; (b) Schematic illustration of the isotope distribution and relative percentages of each peak.

Table 3
Summary of the results of ESI-orbitrap-MS measurement of $^{13}C,^{15}N$-enriched ΔHA_2.

$[M+H]^+$ (m/z)	Measured mass difference (Da)[a]	Expected mass difference (Da)[b]	Isotopologue	Relative percentage (%)
395.1620	0.0000	0.0000	$^{13}C_{14};^{15}N$	37.8
394.1649	−0.9971	−0.9970	$^{13}C_{14};^{14}N$	19.4
394.1595	−1.0025	−1.0034	$^{13}C_{13};^{12}C;^{15}N$	3.2
393.1609	−2.0011	−2.0004	$^{13}C_{13};^{12}C;^{14}N$	1.6
393.1556	−2.0064	−2.0068	$^{13}C_{12};^{12}C_2;^{15}N$	23.1
392.1585	−3.0035	−3.0038	$^{13}C_{12};^{12}C_2;^{14}N$	13.6
392.1533	−3.0087	−3.0102	$^{13}C_{11};^{12}C_3;^{15}N$	1.3
391.1557	−4.0063	−4.0072	$^{13}C_{11};^{12}C_3;^{14}N$	<1
391.1490	−4.0130	−4.0136	$^{13}C_{10};^{12}C_4;^{15}N$	<1

[a] Mass difference from $[M+H]^+ = 395.1620$.
[b] Expected difference to obtain the respective isotopologue.

the *N*-acetyl group was 59–64%. Moreover, combining the percentages of all peaks labeled with ^{15}N yields 65.4% ^{15}N incorporation (37.8% + 3.2% + 23.1% + 1.3%), which agrees well with the average value of amide ^{15}N determined from ^1H NMR spectra.

3. Conclusion

In this work, $^{13}C,^{15}N$-labeled HA polysaccharides were biosynthetically produced by *Streptococcus zooepidemicus* using small-scale cultures and media with defined carbon and nitrogen sources. The HA polymer was enzymatically digested by chondroitinase ABC to the disaccharide repeating unit and the level of ^{13}C and ^{15}N isotope enrichment at each position was determined quantitatively using different types of NMR experiments. The ^{13}C level of the two pyranose rings was determined to be 80–100%, while the ^{13}C and ^{15}N level in the *N*-acetyl group was determined to be 60–65%. These results were further confirmed by high-resolution mass spectrometry. Stable isotope labeling can significantly improve sensitivity and offers the possibility of employing different NMR experiments in carbohydrate research. This work provides an effective method that can be applied to the quantitative assessment of isotopically labeled glycans. As a potential future direction, employing a strictly chemically defined medium to produce uniformly ^{13}C and ^{15}N-labeled HA polysaccharides would help address the issue of isotopic dilution and further enhance detection capabilities by NMR spectroscopy. HA polysaccharides could be submitted to partial enzymatic hydrolysis using chondroitinase or hyaluronidase followed by product separation using HPLC to obtain HA oligosaccharides of defined sizes [40]. The use of size-defined uniformly ^{13}C and ^{15}N-labeled HA oligosaccharides as substrates would greatly facilitate the study of HA-protein interactions and open avenues for comprehensive structure-function analysis in the future.

4. Experimental

4.1. Materials

Chondroitinase ABC from *Proteus vulgaris* (CAS No. 9024-13-9, Product Number: C2905), D-Glucose-$^{13}C_6$ (CAS No. 110187-42-3, Product Number: 389,374) with 99 atom- % ^{13}C, and L-Glutamine-(amide-^{15}N) with 98 atom- %^{15}N (CAS No. 59681-32-2, Product Number: 490,024) were all purchased from Sigma Aldrich (Darmstadt, Germany). *Streptococcus equi* subsp. *Zooepidemicus* strain DSM No. 20727 was purchased from the DSMZ collection (Leibnitz-Institute DSMZ GmbH, Braunschweig, Germany). *N*-[1, 2–$^{13}C_2$] acetyl-D-[UL-$^{13}C_6$; ^{15}N] glucosamine (CAS No. 478529-44-1, Catalog GLC-054) with 99 atom-%^{13}C and 98 atom- %^{15}N was purchased from Omicron Biochemicals, Inc. (South Bend, IN, USA). D_2O (99.96% D) was purchased from Cambridge Isotope Laboratories, Inc. (Tewksbury, MA, USA). Water was

purified with Milli-Q® filtration apparatus (Millipore Co., Bedford, MA, USA).

4.2. Preparation of $^{13}C,^{15}N$-labeled HA polysaccharide

4.2.1. Streptococcus zooepidemicus growth conditions and production of $^{13}C,^{15}N$-labeled HA

Streptococcus equi subsp. *Zooepidemicus* was used in this study for small-scale production of the $^{13}C,^{15}N$-labeled HA. Bacteria were reconstituted from the locally maintained stock. Initially, the bacteria were grown on agar plates, followed by transfer to an inoculation medium (brain heart infusion broth, BHI, ~4 ml) and preincubated for 18 h at 37 °C. The inoculum (~1.5 ml) was then transferred to a liquid culture medium.

For the control set-up, the modified culture medium [41] was prepared. It contained peptone (1 g), yeast extract (0.5 g), L-glutamine (500 mg), and D-glucose (~3.2 g) in a final volume of 100 ml. The control culture with no labeled compounds was done to test the HA preparation procedures. For the metabolic labeling, the D-glucose was replaced by the U–$^{13}C_6$-D-glucose and the L-glutamine was replaced by the L-glutamine-(amide-^{15}N) in the liquid medium.

The liquid cultures were carried out for 24 h at 37 °C, using an incubator shaker operated at 100 rpm with natural aeration. The bacteria were harvested by centrifugation (8000 × g, 30 min) and the supernatant was collected.

4.2.2. Isolation and purification of $^{13}C,^{15}N$-labeled HA polysaccharide

HA polysaccharide was isolated using previously described procedures with modifications [42,43]. Following the separation of bacterial cells, active carbon powder (5.6 g/100 ml) was added and mixed thoroughly with the preserved supernatant. The mixture was incubated for 1 h and filtered. Cold ethanol (96%, stored at −20 °C) was added to the filtrate in a proportion of 1.5:1 (v/v) ethanol/supernatant and incubated at 4 °C, overnight. Subsequently, the white HA precipitate was collected by centrifugation (16,000 × g, 30 min). The precipitation step was repeated thrice. The collected precipitates of HA were freeze-dried. To remove the low-molecular-weight contaminants (medium ingredients and metabolites), the HA fractions were subjected to ultrafiltration (centrifugal filters, cut-off 3 kDa) and the retentate was freeze-dried. In total, a liquid culture of 100 ml yielded ~11.9 mg of $^{13}C,^{15}N$- labeled HA polysaccharide.

4.3. Degradation, separation, and purification

A solution of $^{13}C,^{15}N$-labeled HA polysaccharide (3.5 mg/ml) was prepared in Milli-Q® water, and the pH was adjusted to 7.0 with HCl or NaOH solutions. The aqueous solution was heated to 80 °C for 1 h to aid in the further enzymatic breakdown process. After cooling to room temperature, the HA solution was treated with 0.5 ml of chondroitinase ABC (1.26–12.6 units/ml) at 37 °C for full degradation to disaccharide. The degraded sample was then lyophilized, separated and mass analyzed on a Maxis Impact Q-TOF-MS (Bruker Daltonics GmbH & Co. KG, Bremen, Germany) coupled to a 1290 Infinity II LC system (Agilent Technologies, Santa Clara, CA, USA). The separation was performed across a porous graphite-based Hypercarb™ 4.6 × 100 mm column with a particle size of 3 μm (Thermo Scientific, Waltham, MA, USA) kept at 40 °C. The mobile phases employed were (A) water and (B) acetonitrile, both containing 0.05% trifluoroacetic acid, and a flow rate of 0.5 ml/min was used. A linear gradient from 20 to 40% mobile phase B in 15 min followed by a 5 min wash step with 20% mobile phase B was used. The MS was operated in the full scan positive ion mode. The α and β anomers of the disaccharide could be well separated as two chromatographic peaks and were identified from their labeled protonated molecular ion clusters. The same protocol was used to fractionate the two peaks on a micro-scale. A post-column splitter at the entrance to the MS was used to collect the eluents from several injections (20 μl each). The

pooled eluents were combined, lyophilized, and subjected to further analyses.

4.4. ESI-orbitrap-MS

The high-resolution capability of the Orbitrap QExactive mass spectrometer (Thermo Fisher Scientific) was exploited to obtain the spectra depicted in Fig. 6a. The chromatographic separation was performed on a Vanquish Horizon UHPLC system (Thermo Fisher Scientific) having a porous graphite-based Hypercarb™ 4.6 × 100 mm column with a particle size of 3 μm (Thermo Scientific, Waltham, MA, USA), maintained at a temperature of 40 °C. The mobile phases employed were (A) water and (B) acetonitrile, both containing 0.2% formic acid, and a flow rate of 0.5 ml/min was used. A linear gradient from 20 to 40% mobile phase B in 15 min followed by a 5-min wash step with 20% mobile phase B was used. The QExactive HF mass spectrometer was operated in the full scan positive ion mode (scan 70–1050 Da) with a spray voltage of 3.5 kV, a capillary temperature of 350 °C, and sheath and aux pressures of 50 and 15 arbitrary units respectively. Profile MS spectra were obtained at a resolution of 240,000 and an auto-gain control target of 3×10^6.

4.5. NMR spectroscopy

The freeze-dried disaccharide sample was dissolved in 160 μl 90% H_2O/10% D_2O and transferred into a 3 mm NMR sample tube. NMR spectra were recorded on a Bruker Avance III 600 MHz spectrometer using a 5 mm $^1H/^{13}C/^{15}N/^{31}P$ inverse detection CryoProbe equipped with a z-gradient (Bruker BioSpin GmBH, Ettlingen, Germany). The chemical shifts for NMR signals were referenced by using DSS-d_6 as an internal reference (δ_H 0.0 ppm δ_C 0.0 ppm). NMR spectra were processed with TopSpin 4.0.6 (Bruker). The ^1H NMR spectra were recorded using the pulse sequences *zgesgp, noesygppr1d, ledbpgp2s1d* and *zggpw5* from the Bruker pulse sequence library. ^{13}C- or ^{15}N-decoupled spectra were acquired with a modified excitation sculpting pulse sequense (*zgesgp*) with decoupling during the acquisition time, which was limited to 0.85 s. Decoupling was obtained with the GARP-4 decoupling sequence, using a pulse length of 148.3 μs for ^{13}C decoupling (equivalent to a bandwidth of 9.3 kHz) and 547.5 μs for ^{15}N decoupling (equivalent to a bandwidth of 2.5 kHz). The ^{15}N decoupling was centered at 120 ppm and the ^{13}C decoupling was centered at 30 and 110 ppm for decoupling of methyl and G4 carbons, respectively. To obtain quantitative ^1H spectra, the relaxation delay (D1) was set to at least 25 s. Phase correction, baseline correction, and line broadening with a factor of 0.3 Hz were conducted prior to peak integration of the ^1H NMR signals. Quantitative 1D ^{13}C spectra were recorded with the inverse-gated decoupling experiment *zgig30* from the Bruker pulse sequence library with a relaxation delay (D1) of 25 s and 16 k scans. A spectral width of 240 ppm and an acquisition time of 0.9 s was applied. Automatic baseline correction was performed with the command *c13cryo*. Phase correction and a line broadening factor of 5 Hz were used prior to peak integration. Quantitative 2D ^1H, ^{13}C-HSQC spectra (*hsqcetgpsp.3* from Bruker pulse sequence library) were recorded with 1 k data points in t₂ and 256 increments in t₁, 16 dummy scans, 32 scans, and 5–20 s relaxation delay. A spectral width of 8 ppm in F₂ and 120 ppm in F₁ was used and the transmitter offset was set at 4.7 ppm in F₂ and 62 ppm in F₁. The integration of 2D peak volumes was performed after a 90° shifted squared sine bell function and automatic baseline correction in both dimensions. 2D ^1H,^{13}C-HMBC and ^1H, ^{15}N-HSQC (*hmbcctetgpnd* and *fhsqcf3gpph* from the Bruker pulse sequence library)* spectra were recorded with 2 k data points in t₂ and 128 to 256 increments in t₁, with a minimum of 16 scans per increment and a relaxation delay of 1.0–1.2 s ^{13}C T_1 was determined from an inversion recovery experiment (*t1irpg* from the Bruker pulse sequence library)* after a relaxation delay of 30 s. A variable delay list of 9 points between 0.05 and 30 s was used. 16 scans were recorded for each point.

Declaration of competing interest

The authors declare that they have no known competing financial interests or personal relationships that could have appeared to influence the work reported in this paper.

Data availability

Data will be made available on request.

Appendix A. Supplementary data

Supplementary data to this article can be found online at https://doi.org/10.1016/j.carres.2023.108888.

References

[1] I. Hargittai, M. Hargittai, Molecular structure of hyaluronan: an introduction, Struct. Chem. 19 (2008) 697–717, https://doi.org/10.1007/s11224-008-9370-3.

[2] A. Lierova, J. Kasparova, A. Filipova, J. Cizkova, L. Pekarova, L. Korecka, N. Mannova, Z. Bilkova, Z. Sinkorova, Hyaluronic acid: known for almost a century, but still in vogue, Pharmaceutics 14 (2022) 838, https://doi.org/10.3390/pharmaceutics14040838.

[3] K.T. Dicker, L.A. Gurski, S. Pradhan-Bhatt, R.L. Witt, M.C. Farach-Carson, X. Jia, Hyaluronan: a simple polysaccharide with diverse biological functions, Acta Biomater. 10 (2014) 1558–1570, https://doi.org/10.1016/j.actbio.2013.12.019.

[4] M.K. Cowman, Hyaluronan and hyaluronan fragments, Adv. Carbohydr. Chem. Biochem. 74 (2017) 1–59, https://doi.org/10.1016/bs.accb.2017.10.001.

[5] S. Garantziotis, R.C. Savani, Hyaluronan biology: a complex balancing act of structure, function, location and context, Matrix Biol. 78 (2019) 1–10, https://doi.org/10.1016/j.matbio.2019.02.002.

[6] T.N. Wight, Provisional matrix: a role for versican and hyaluronan, Matrix Biol. 60 (2017) 38–56, https://doi.org/10.1016/j.matbio.2016.12.001.

[7] J.E. Rayahin, J.S. Buhrman, Y. Zhang, T.J. Koh, R.A. Gemeinhart, High and low molecular weight hyaluronic acid differentially influence macrophage activation, ACS Biomater. Sci. Eng. 1 (2015) 481–493, https://doi.org/10.1021/acsbiomaterials.5b00181.

[8] O. Guvench, Atomic-resolution experimental structural biology and molecular dynamics simulations of hyaluronan and its complexes, Molecules 27 (2022) 7276, https://doi.org/10.3390/molecules27217276.

[9] M.D. Battistel, D.I. Freedberg, Dispersing the crowd: adopting 13C direct detection for glycans, J. Magn. Reson. 318 (2020), 106792, https://doi.org/10.1016/j.jmr.2020.106792.

[10] L. Paudel, R.W. Adams, P. Király, J.A. Aguilar, M. Foroozandeh, M.J. Cliff, M. Nilsson, P. Sándor, J.P. Waltho, G.A. Morris, Simultaneously enhancing spectral resolution and sensitivity in heteronuclear correlation NMR spectroscopy, Angew. Chem., Int. Ed. Engl. 52 (2013) 11616–11619, https://doi.org/10.1002/anie.201305709.

[11] G. Nestor, T. Anderson, S. Oscarson, A.M. Gronenborn, Exploiting uniformly 13C-labeled carbohydrates for probing carbohydrate–protein interactions by NMR spectroscopy, J. Am. Chem. Soc. 139 (2017) 6210–6216, https://doi.org/10.1021/jacs.7b01929.

[12] A. Gimeno, P. Valverde, A. Ardá, J. Jiménez-Barbero, Glycan structures and their interactions with proteins. A NMR view, Curr. Opin. Struct. Biol. 62 (2020) 22–30, https://doi.org/10.1016/j.sbi.2019.11.004.

[13] G. Nestor, T. Anderson, S. Oscarson, A.M. Gronenborn, Direct observation of carbohydrate hydroxyl protons in hydrogen bonds with a protein, J. Am. Chem. Soc. 140 (2018) 339–345, https://doi.org/10.1021/jacs.7b10595.

[14] J. Orts, A.D. Gossert, Structure determination of protein-ligand complexes by NMR in solution, Methods 138–139 (2018) 3–25, https://doi.org/10.1016/j.ymeth.2018.01.019.

[15] C. Dominguez, M. Schubert, O. Duss, S. Ravindranathan, F.H.-T. Allain, Structure determination and dynamics of protein–RNA complexes by NMR spectroscopy, Prog. Nucl. Magn. Reson. Spectrosc. 58 (2011) 1–61, https://doi.org/10.1016/j.pnmrs.2010.10.001.

[16] M. Schubert, Insights into carbohydrate recognition by 3D structure determination of protein–carbohydrate complexes using NMR. https://doi.org/10.1039/9781782623946-00101, 2017.

[17] Z. Zhang, S.A. McCallum, J. Xie, L. Nieto, F. Corzana, J. Jiménez-Barbero, M. Chen, J. Liu, R.J. Linhardt, Solution structures of chemoenzymatically synthesized heparin and its precursors, J. Am. Chem. Soc. 130 (2008) 12998–13007, https://doi.org/10.1021/ja8026345.

[18] C. Sigulinsky, P. Babu, X.V. Victor, B. Kuberan, Preparation and characterization of 15N-enriched, size-defined heparan sulfate precursor oligosaccharides, Carbohydr. Res. 345 (2010) 250–256, https://doi.org/10.1016/j.carres.2009.10.024.

[19] T.K.N. Nguyen, Characterization of uniformly and atom-specifically 13C-labeled heparin and heparan sulfate polysaccharide precursors using 13C NMR spectroscopy and ESI mass spectrometry, Carbohydr. Res. 345 (2010) 2228–2232, https://doi.org/10.1016/j.carres.2010.08.011.

[20] B.M. Sattelle, J. Shakeri, I.S. Roberts, A. Almond, A 3D-structural model of unsulfated chondroitin from high-field NMR: 4-sulfation has little effect on

backbone conformation, Carbohydr. Res. 345 (2010) 291–302, https://doi.org/10.1016/j.carres.2009.11.013.

[21] V.H. Pomin, J.S. Sharp, X. Li, L. Wang, J.H. Prestegard, Characterization of glycosaminoglycans by 15N NMR spectroscopy and in vivo isotopic labeling, Anal. Chem. 82 (2010) 4078–4088, https://doi.org/10.1021/ac1001383.

[22] A.W. Barb, D.I. Freedberg, M.D. Battistel, J.H. Prestegard, NMR detection and characterization of sialylated glycoproteins and cell surface polysaccharides, J. Biomol. NMR 51 (2011) 163–171, https://doi.org/10.1007/s10858-011-9550-0.

[23] C. Blundell, P. Deangelis, A.J. Day, A. Almond, Use of 15N-NMR to resolve molecular details in isotopically-enriched carbohydrates: sequence-specific observations in hyaluronan oligomers up to decasaccharides, Glycobiology 14 (2004) 999–1009, https://doi.org/10.1093/GLYCOB/CWH117.

[24] M. Mobli, M. Nilsson, A. Almond, The structural plasticity of heparan sulfate NA-domains and hence their role in mediating multivalent interactions is confirmed by high-accuracy (15)N-NMR relaxation studies, Glycoconj. J. 25 (2008) 401–414, https://doi.org/10.1007/s10719-007-9081-9.

[25] S.C. Namboori, D.E. Graham, Acetamido sugar biosynthesis in the euryarchaea, J. Bacteriol. 190.8 (2008) 2987–2996.

[26] B.F. Chong, L.M. Blank, R. Mclaughlin, L.K. Nielsen, Microbial hyaluronic acid production, Appl. Microbiol. Biotechnol. 66 (2005) 341–351, https://doi.org/10.1007/s00253-004-1774-4.

[27] B.F. Chong, L.K. Nielsen, Amplifying the cellular reduction potential of Streptococcus zooepidemicus, J. Biotechnol. 100 (2003) 33–41, https://doi.org/10.1016/s0168-1656(02)00239-0.

[28] T. Yamagata, H. Saito, O. Habuchi, S. Suzuki, Purification and properties of bacterial chondroitinases and chondrosulfatases, J. Biol. Chem. 243 (1968) 1523–1535, https://doi.org/10.1016/S0021-9258(18)93574-X.

[29] A. Hamai, N. Hashimoto, H. Mochizuki, F. Kato, Y. Makiguchi, K. Horie, S. Suzuki, Two distinct chondroitin sulfate ABC lyases: an endoeliminase yielding tetrasaccharides and an exoeliminase preferentially acting on oligosaccharides, J. Biol. Chem. 272 (1997) 9123–9130, https://doi.org/10.1074/jbc.272.14.9123.

[30] C.D. Blundell, M.A.C. Reed, A. Almond, Complete assignment of hyaluronan oligosaccharides up to hexasaccharides, Carbohydr. Res. 341 (2006) 2803–2815, https://doi.org/10.1016/j.carres.2006.09.023.

[31] G. Nestor, L. Kenne, C. Sandström, Experimental evidence of chemical exchange over the β(1→3) glycosidic linkage and hydrogen bonding involving hydroxy protons in hyaluronan oligosaccharides by NMR spectroscopy, Org. Biomol. Chem. 8 (2010) 2795, https://doi.org/10.1039/b927159g.

[32] M.K. Cowman, J. Feder-Davis, D.M. Hittner, 13C NMR studies of hyaluronan. 2. Dependence of conformational dynamics on chain length and solvent, Macromolecules 34 (2001) 110–115, https://doi.org/10.1021/ma001082e.

[33] A. Donati, A. Magnani, C. Bonechi, R. Barbucci, C. Rossi, Solution structure of hyaluronic acid oligomers by experimental and theoretical NMR, and molecular dynamics simulation, Biopolymers 59 (2001) 434–445, https://doi.org/10.1002/1097-0282(200111)59:6<434::AID-BIP1048>3.0.CO;2-4.

[34] H. Hofmann, O. Schmut, H. Sterk, H. Pölzler, Relaxation time measurements of hyaluronic acid, J. Biol. Macromol. 5.4 (1983) 229–232, https://doi.org/10.1016/0141-8130(83)90007-7.

[35] P. Giraudeau, Challenges and perspectives in quantitative NMR, Magn. Reson. Chem. 55 (2017) 61–69, https://doi.org/10.1002/mrc.4475.

[36] H. Koskela, Annual Reports on NMR Spectroscopy, Chapter 1 Quantitative 2D NMR Studies, vol. 66, Academic Press, 2009, pp. 1–31, https://doi.org/10.1016/S0066-4103(08)00401-8.

[37] L. Zhang, G. Gellerstedt, Quantitative 2D HSQC NMR determination of polymer structures by selecting suitable internal standard references, Magn. Reson. Chem. 45 (2007) 37–45, https://doi.org/10.1002/mrc.1914.

[38] D. Lane, T.E. Skinner, N.I. Gershenzon, W. Bermel, R. Soong, R. Dutta Majumdar, Y. Liaghati Mobarhan, S. Schmidt, H. Heumann, M. Monette, M.J. Simpson, A. J. Simpson, Assessing the potential of quantitative 2D HSQC NMR in 13C enriched living organisms, J. Biomol. NMR 73 (2019) 31–42, https://doi.org/10.1007/s10858-018-0221-2.

[39] L. Liu, Y. Liu, J. Li, G. Du, J. Chen, Microbial production of hyaluronic acid: current state, challenges, and perspectives, Microb. Cell Factories 10 (2011) 99, https://doi.org/10.1186/1475-2859-10-99.

[40] A. Tawada, T. Masa, Y. Oonuki, A. Watanabe, Y. Matsuzaki, A. Asari, Large-scale preparation, purification, and characterization of hyaluronan oligosaccharides from 4-mers to 52-mers, Glycobiology 12 (2002) 421–426, https://doi.org/10.1093/glycob/cwf048.

[41] C. Matsubara, M. Kajiwara, H. Akasaka, S. Haze, Carbon-13 nuclear magnetic resonance studies of the biosynthesis of hyaluronic acid, Chem. Pharm. Bull. 39 (1991) 2446–2448, https://doi.org/10.1248/cpb.39.2446.

[42] A.M.B. Pires, M.H.A. Santana, Metabolic effects of the initial glucose concentration on microbial production of hyaluronic acid, Appl. Biochem. Biotechnol. 162 (2010) 1751–1761, https://doi.org/10.1007/s12010-010-8956-6.

[43] V. Rangaswamy, D. Jain, An efficient process for production and purification of hyaluronic acid from Streptococcus equi subsp, zooepidemicus, Biotechnol. Lett. 30 (2008) 493–496, https://doi.org/10.1007/s10529-007-9562-8.